PCCP

PAPER

View Article Online
View Journal | View Issue

Cite this: *Phys. Chem. Chem. Phys.*, 2017, **19**, 10913

Transformation of PbI_2, $PbBr_2$ and $PbCl_2$ salts into $MAPbBr_3$ perovskite by halide exchange as an effective method for recombination reduction†

Eya Belarbi,[ab] Marta Vallés-Pelarda,[a] Bruno Clasen Hames,[a] Rafael S. Sanchez,[a] Eva M. Barea,[a] Hager Maghraoui-Meherzi[b] and Iván Mora-Seró *[a]

Received 22nd February 2017,
Accepted 30th March 2017

DOI: 10.1039/c7cp01192j

rsc.li/pccp

Halide perovskite derivatives present unprecedented physical phenomena among those materials which are suitable for photovoltaics, such as a fast ion diffusion coefficient. In this paper it is reported how the benefits of this property can be used during the growth of halide perovskites in order to control the morphological and optoelectronic properties of the final thin film. Using a large enough halide reservoir, the nature of the halides present in the final perovskite layer can be exchanged and this depends on the initial salt used in the two-step deposition method. In particular, the preparation of a methylammonium lead bromide ($MAPbBr_3$) thin film is reported, using a two-step method based on the transformation of lead(II) iodide (PbI_2), lead(II) bromide ($PbBr_2$) and lead(II) chloride ($PbCl_2$) salts into $MAPbBr_3$ perovskite after dipping in a methylammonium bromide (MABr) solution. The films prepared from different salts present different properties in terms of morphology and optoelectronic properties, thus providing significantly different performance when they are used for the preparation of photovoltaic devices. Interestingly, the use of PbI_2 and $PbCl_2$ salts reduce the charge recombination and increase the open circuit potential obtained, especially in the former case. However, the highest photocurrent is obtained when $PbBr_2$ is used. For PbI_2 and $PbCl_2$ salts no traces of the former salt are observed in the $MAPbBr_3$ layer obtained after 10 minutes of dipping time, however, the presence of $PbBr_2$ has still been detected (using X-ray diffraction) when this salt has been employed.

Introduction

Halide perovskite solar cells (PSCs) have attracted a great amount of attention in the last few years because of their excellent properties for the development of highly efficient opto-electronic devices using relatively simple methodologies.[1–3] Halide perovskites present an ABX_3 structure, where A is a small organic cation (*e.g.*, $CH_3NH_3^+ = MA^+$) or inorganic [cesium ions (Cs^+) or rubidium ions (Rb^+)], B is a divalent metal cation [*e.g.*, lead ions (Pb^{2+}) which is the one used most extensively] and X is a halide ion [iodide (I^-), chloride (Cl^-), bromide (Br^-)].[4–6] The versatility, in terms of chemical composition, makes the halide perovskites an extremely interesting family of materials. Their properties, such as bandgap, which can be tuned with appropriate composition control, increase the range of applications to beyond conventional photovoltaics. For example, large bandgap halide perovskites,[7,8] using Br^- instead of I^-, can be used as the top cell in tandem devices.[9,10] Furthermore, the capability of tuning the bandgap along all the visible range, with the appropriate ratio of halides, also makes the same materials extremely interesting for light emitting systems.[11,12]

Since the first reports on all solid PSCs,[13,14] different fabrication methods have shown that is possible to obtain high quality halide perovskite thin films, but probably, the most extensively used methods are based on the spin coating deposition of the precursor solutions. The first reported methods where the perovskite film was fabricated through a single spin coating step from a solution containing all the perovskite precursors. Very early on it was observed that the precursors have a strong influence on the final thin film properties and consequently, on the device performance later on. For example the substitution of lead(II) iodide (PbI_2), totally or partially, by lead(II) chloride ($PbCl_2$) has an important effect on the methylammonium lead halide ($MAPbI_3$) film morphology but also on the optoelectronic

[a] *Institute of Advanced Materials (INAM), Universitat Jaume I, 12006 Castelló, Spain. E-mail: sero@uji.es*
[b] *Université de Tunis El Manar, Faculté des Sciences de Tunis, Laboratoire de Chimie Analytique et d'Électrochimie LR99ES15, Campus Universitaire de Tunis El Manar 2092, Tunis, Tunisia*

† Electronic supplementary information (ESI) available: Comparison of the diffraction angle 2θ from the perovskite (100) planes measured at different dipping times. Energy-dispersive X-ray (EDX) analysis. Light absorption and normalized photoluminescence spectra of the different samples analyzed. See DOI: 10.1039/c7cp01192j

properties.[15–21] The incorporation of Cl^- in the film was under the detection limit or, in those cases in which it was able to be measured, is lower than 2%.[17,19] Similar behavior has been observed when $PbCl_2$ was used instead of lead(II) bromide ($PbBr_2$) for the formation of methylammonium lead bromide ($MAPbBr_3$).[7,20] Consequently, it was realised that the halogen precursor plays a dramatic role on the properties of the film.

Furthermore, results from experiments on halide perovskites points to a high mobility of the halide ions. This property has been used to control the halogen content of nanoparticles $CsPbX_3$ (X = I, Br, Cl or a combination of these halides), thus transforming a nanoparticle originally containing a specific halogen into a nanoparticle with a different halogen composition.[22–24] This halide exchange is especially useful to preserve the perovskite structure for compounds that can present several crystalline phases [*i.e.*, cesium lead iodide ($CsPbI_3$)].[23] Halide exchange has also been used to transform $MAPbX_3$ films using both gas treatment under halide atmosphere,[25,26] or by dipping into a MAX solution.[27] In both these cases, the starting $MAPbX_3$ film acts as a template and therefore, the perovskite obtained after the halide exchange presents the same crystalline phase as its initial one even though the halide composition has been altered. The studies focused on halide exchange found in the literature mainly tackle the effect of the halide on the structural modifications, with limited analysis of the implications of the performance of the devices. Pellet *et al.* observed that $MAPbX_3$ films produced by halide exchange presented a higher photoluminescence (PL) than those films originally prepared with a $MAPbX_3$ composition, but no devices were characterized.[27] Li *et al.* observed an increase in the photovoltaic conversion efficiency for those samples prepared with perovskite after halide exchange, but no further characterization of devices was performed.[25]

The research presented here reports on the preparation of $MAPbBr_3$ perovskite layers from PbI_2, $PbBr_2$ or $PbCl_2$ films. After a lengthy dip in a methylammonium bromide (MABr) solution, the lead halide films were transformed into perovskite and it is worth mentioning that MA^+ was quickly incorporated into the layer, whereas halide exchange required a longer diffusion time. Finally, all three salt layers were transformed into $MAPbBr_3$ layers as has been demonstrated through PL measurements and X-ray diffraction (XRD). This transformation presents a significant difference to transformations reported in previous papers. In previous research the halide exchange was produced when a perovskite layer was already formed,[25–27] and consequently the process just needed the migration of halide anions, whereas the two-step process reported here needed in addition the migration of the MA cation. Interestingly the structural, optical and electrical properties of the final films were strongly influenced by the initial salt used for the perovskite synthesis and this has important implications for the ultimate performance of PSCs, as has been systematically determined using scanning electron microscopy (SEM), energy-dispersive X-ray (EDX) spectroscopy, light absorption measurements, PL, XRD, current–potential (*J*–*V*) curves and impedance spectroscopy (IS). The previous characterization of perovskite layers produced by halide exchange has focused on the structural properties of the films with very few examples of solar cell preparation,[25] and even in this case there was not an indepth analysis of the origin of the differences observed among samples prepared by halide exchange. Conversely, the general characterization carried out in this research has allowed the understanding of the different solar cell behavior of photovoltaic devices prepared with $MAPbBr_3$, correlating the solar cell performance with the structural properties of the different layers.

Experimental

Deposition of c-TiO_2 and mp-TiO_2

Fluorine doped tin oxide (FTO) coated glass substrates (25 × 25 mm, Pilkington TEC 15, ~15 Ω sq^{-1} resistance) were partially etched using a chemical treatment with zinc powder and hydrochloric acid (2 M), cleaned with soap (Hellmanex) and rinsed with Milli-Q water. Then, the substrates were cleaned ultrasonically in a mixture of acetone/ethanol (1 : 1 v/v) for 15 min and then dried with compressed air. To remove all the water vapor, they were heated up to 80 °C for 30 min and finally treated in an ultraviolet (UV)-ozone chamber for 10 min before use. The compact titanium dioxide (c-TiO_2) layer was deposited on the top of the substrates using a manual spray pyrolysis at 450 °C with 5 mL of a titanium diisopropoxide bis(acetylacetonate) solution (75% in 2-propanol, Sigma-Aldrich) that was diluted in absolute ethanol (0.5 : 4.5 v/v). Compressed oxygen was used as the carrier gas. The spraying of the titanium precursor solution was performed in three steps of 6 s each with an interval of 30 s between each step. After spraying all the precursor solution, the films were kept at 450 °C for 30 min.

The mesoporous spherical TiO_2 (ms-TiO_2) layer was spin coated (2000 rpm, 10 s) using 100 μL of a solution of a TiO_2 paste (30 NR-D, Dyesol, 30 nm average particle size) diluted in absolute ethanol (1 : 5 v/v). Then the films were dried on a hotplate at 100 °C for 10 min, heated up to 500 °C for 30 min and finally, cooled down at room temperature. All the samples analyzed in this work have the same substrate configuration: glass/FTO/c-TiO_2/ms-TiO_2.

PSC fabrication

The perovskite layers were prepared using a two-step method. It is worth noting that PbI_2, $PbBr_2$, and $PbCl_2$, were employed for the fabrication of the perovskite (PS) films. $PbBr_2$ (1 M) (99.99%, TCI Chemicals) and PbI_2 (1 M) (99.99%, TCI Chemicals) were independently dissolved in *N*,*N*-dimethylformamide (DMF). However, $PbCl_2$ (1 M) (99.99%, Aldrich) was dissolved in a mixture of solvents DMF/dimethylsulfoxide (7 : 3 v/v). All the lead precursor solutions were kept at 70 °C for 30 min under stirring. After complete dissolution, 30 μL of each one was spin coated over all the substrate (500 rpm for 5 s and 6000 rpm for 20 s). Then, the films were heated for 3 min at 40 °C and 10 min at 100 °C. Subsequently, the films were dipped into a 10 mg mL^{-1} solution of MABr in 2-propanol (98%, Aldrich) for

different reaction times (40 s, 1 min, 5 min or 10 min), then rinsed with 2-propanol and dried at 100 °C for 10 min.

The Spiro-OMeTAD layer was dynamically spin coated onto the FTO/c-TiO_2/mp-TiO_2/$MAPbBr_3$ substrate (4000 rpm for 30 s). The Spiro-OMeTAD solution was prepared by dissolving 72.3 mg of (2,2′,7,7′-tetrakis(*N*,*N*′-di-*p*-methoxyphenylamine)-9,9′-spirobifluorene), 28.8 μL of 4-*t*-butylpyridine and 17.5 μL of a stock solution of lithium bis(trifluoromethylsulfonyl)imide (520 mg mL^{-1} of the lithium salt in acetonitrile) in 1 mL of chlorobenzene. Finally, 100 nm of gold (Au) was thermally evaporated on the top of the devices to form the metal contact.

Characterization of the perovskite films

The structural properties of the PS films were examined using XRD with a Bruker AXS, D4 Endeavor advanced X-ray diffractometer using Cu Kα radiation. The surface morphologies were determined using SEM with a Jeol, JEM-3100F field emission gun scanning electron microscope (FEG-SEM) including EDX analysis. The optical properties of these perovskite films were studied using ultraviolet-visible (UV-vis) spectroscopy using a Varian Cary 300 Bio spectrophotometer and the PL spectra were obtained using a Horiba FL-1000 fluorimeter. IS was performed using a Metrohm Autolab PGSTAT30 potentiostat under chopped light. *J–V* curves of the PSCs were measured under 1 Sun conditions (100 mW cm^{-2}, AM 1.5G) using a solar simulator from Abet technologies.

Results and discussion

The transformation of the PbI_2, $PbBr_2$ or $PbCl_2$ layer into $MAPbBr_3$ by dipping the samples in a solution of MABr is produced by the incorporation of MA^+ cations at the same time that Cl^- and I^- anions are exchanged by Br^- anions. PbX_2 films were dipped into a solution of MABr with a concentration of 10 mg mL^{-1}. The effect of the reaction time on the properties of the PbX_2 salt films was determined by characterizing the films after different dipping times: 40 s, 1 min, 5 min and 10 min. Fig. 1 shows the results of a qualitative analysis of the transformation by just comparing the color evolution of the different salt layers with the dipping time. $PbCl_2$ and $PbBr_2$ films are colorless, whereas the PbI_2 films show a strong yellow coloration. After dipping PbX_2 films, very different color evolution was observed depending on the original PbX_2 layer, however, a very similar deep yellow coloration was obtained after 10 minutes of dipping time for all the samples. Whereas the $PbBr_2$ films acquire the final coloration after just 40 s of reaction, the colorless $PbCl_2$ acquires it more slowly. On the contrary, the PbI_2 film initially turned orange, but upon longer exposure to the MABr solution, the film gradually became a deep yellow color.

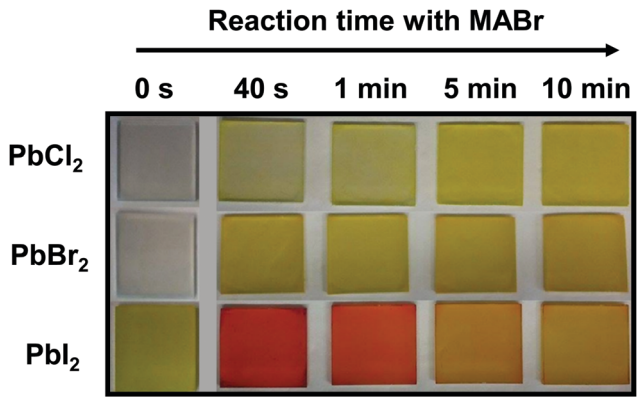

Fig. 1 Photograph of the lead halide precursor films (0 s) and of the films after 40 s, 1 min, 5 min and 10 min of dipping time in a 10 mg mL^{-1} solution of MABr in 2-propanol, then rinsed with 2-propanol and dried at 100 °C for 10 min.

Fig. 2 shows the XRD patterns of the original PbX_2 films and of the same films exposed to MABr solution with different dipping times. After 10 min of dipping time the XRD spectra is dominated in all the cases by the diffraction peak of the planes (100) of the crystalline structure corresponding to $MAPbBr_3$ with a small angle deviation on the main peak ($2\theta \approx 14.96°$) that arises from the different lead halide precursors used. The presence of this peak and those corresponding to other diffractions of $MAPbBr_3$ indicate the formation of the bromide perovskite in all three cases after 10 min of dipping time, see Fig. 2. The characteristic diffraction peaks of the $MAPbBr_3$ were ascribed to the crystal planes (100), (200) and (300) at 14.96°, 30.14° and 45.9°, respectively.[28]

When $PbBr_2$ was used as the lead precursor the intensity of the diffraction peak (100) from $MAPbBr_3$ increases progressively with the dipping time, see the inset in Fig. 2b. However, after 10 min of reaction, in addition to the diffraction peaks from $MAPbBr_3$, those diffraction peaks corresponding to $PbBr_2$, (022), (111), (021), or (112) were still visible, thus indicating that the transformation from $PbBr_2$ into $MAPbBr_3$ is not totally completed after 10 min and a mixed phase is obtained, in which $PbBr_2$ is still present. This fact indicated a diffusion limitation of MA though the $PbBr_2$ salt. Interestingly, $MAPbBr_3$ is quickly formed when PbI_2 is used, as can be recognized by the clear diffraction peak from the $MAPbBr_3$ (100) planes after just 40 s of dipping time, see the inset in Fig. 2a. Note that no trace of $MAPbI_3$, characterized by the (110) diffraction peak at $2\theta = 14.12°$, can be found, see inset in Fig. 2a. This fact indicates that the $MAPbBr_3$ phase is significantly dominant compared to other possible phases not detected using XRD. At the same time, those peaks from PbI_2 have practically disappeared after this short dipping time, as can be found from the strong decrease of diffraction from the PbI_2(005) planes. After 10 minutes of dipping time no trace of PbI_2 is present in the XRD spectra and a total transformation into $MAPbBr_3$ was produced. In contrast to the $PbBr_2$ salt the diffusion of MA though the PbI_2 salt does not present a severe limitation.

For the $PbCl_2$ layer, as in the case of PbI_2 and in contrast with $PbBr_2$, no peaks from the original salt are observed after 10 min of dipping time, see Fig. 2c. After 10 minutes of dipping time the diffraction peak from the perovskite (100) plane was detected at 14.92° for those samples prepared from PbI_2 and $PbBr_2$, and at 14.96° for the sample starting from $PbCl_2$, see the insets in Fig. 2 and these values can be considered to be equal when the experimental error was taken into account,

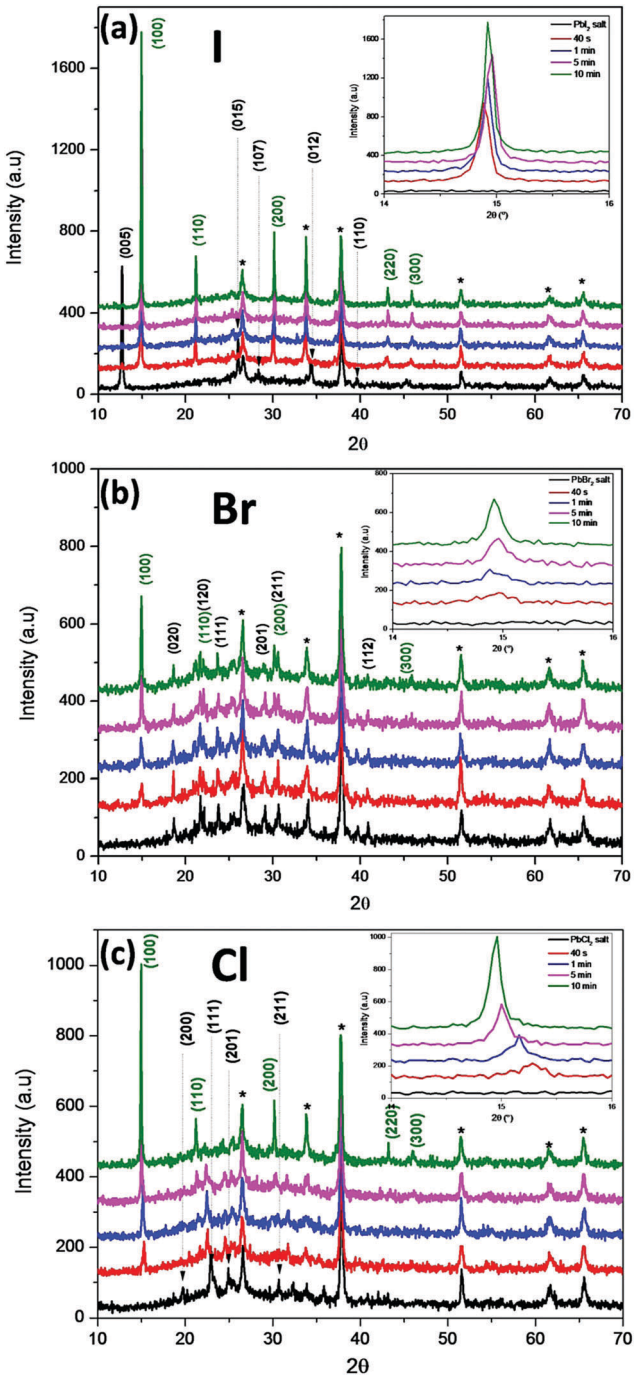

Fig. 2 XRD patterns of $MAPbBr_3$ and PbX_2 films starting from three different lead salts, (a) PbI_2, (b) $PbBr_2$ and (c) $PbCl_2$. Diffraction peaks from the FTO substrate are indicated with asterisks. Green labels indicate the diffraction planes corresponding to $MAPbBr_3$ whereas black labels indicate the diffraction planes corresponding to PbX_2. The insets show a magnified plot of the 2θ region of the diffracting (100) peak from $MAPbBr_3$.

see Fig. S1 (ESI†). However, the evolution of the position of this peak depends strongly on the initial PbX_2 salt, whereas for PbI_2 and $PbBr_2$ the position of the (100) signal does not significantly shift over the dipping time. However, for the $PbCl_2$ sample a clear evolution from larger to smaller 2θ values is observed over the reaction time, see inset Fig. 2c and Fig. S1 (ESI†).

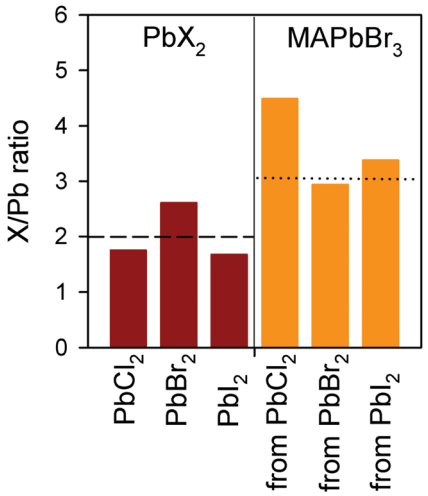

Fig. 3 X/Pb atomic ratio obtained using the EDX measurements [see Fig. S2 (ESI†) for more details] using different halides, where X = Cl, Br or I. On the left hand side is the ratio obtained for the original PbX_2 salts, whereas on the right hand side is the measured ratio of the final $MAPbBr_3$ layer. The black dashed and dotted lines are eye guides indicating the stoichiometric ratio for the salts and for the perovskite, 2 and 3, respectively.

This behavior indicates that for PbI_2 and $PbBr_2$ salts, the $MAPbBr_3$ is quickly formed whereas for $PbCl_2$ first the $MAPbCl_3$ is formed, and this is characterized by the (100) diffraction peak at $2\theta = 15.22^\circ$, see inset in Fig. 2c. As the dipping time increases a mixed $MAPb(Cl_xBr_{1-x})_3$ perovskite is formed, as can be observed by the shift to lower 2θ diffraction angles of the (100) diffraction peak. The x values decrease with the dipping time until the $MAPbBr_3$ perovskite is finally formed after 10 minutes of dipping time.

From the XRD measurements it can be concluded that independently of the PbX_2 halide salt used as original layer, $MAPbBr_3$ was obtained after a 10 minute dipping process, as has already been commented on. However, unexpectedly just for the samples starting from a $PbBr_2$ layer, the salt phase is not totally removed. In order to explain this unexpected result EDX spectroscopy was carried out on the original PbX_2 salt layers and on the finally transformed $MAPbBr_3$, obtained after 10 minutes dipping, see Fig. S2 (ESI†). The EDX results obtained were in good agreement with those obtained using XRD and there was no trace of I or Cl in the $MAPbBr_3$ films detected above the detection threshold of the equipment, see Fig. S2 (ESI†). The X/Pb atomic ratio obtained from the EDX measurements is plotted in Fig. 3. Note that $PbBr_2$ is a halide rich film whereas $PbCl_2$ and PbI_2 are lead rich films, and consequently have a high density of halide vacancies. The halide vacancies allow the fast incorporation of Cl and I into the film structure during the dipping process and as has been shown previously halogen migration is mainly ruled by the vacancies.[29,30] However, in Pb rich perovskite the punctual defect with the lowest formation energy is the presence of MA in an interstitial position,[31] which allows the fast incorporation of MA ions into the structure of Pb rich $PbCl_2$ and PbI_2. However, for the halide rich layer the formation energy of these defects is higher making this

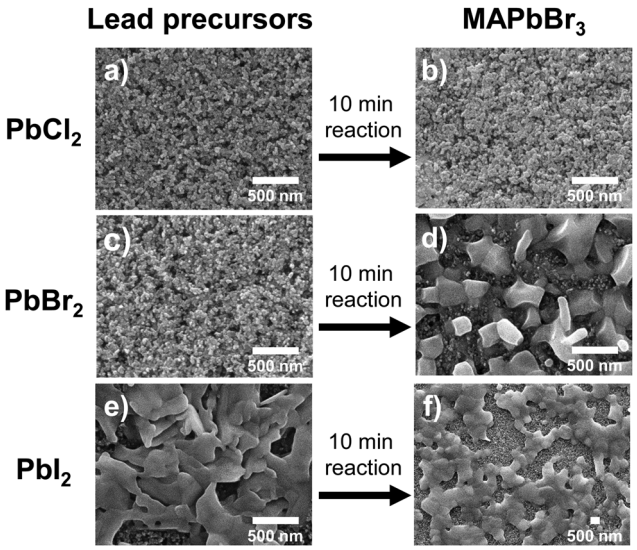

Fig. 4 Top view SEM images of the films shown in Fig. 1. Lead halide precursors (a, c and e) and the corresponding perovskite films after reaction by dipping in a MABr solution in 2-propanol for 10 min (b, d and f). All the films were deposited on the top of FTO/c-TiO_2/mp-TiO_2.

incorporation more difficult. Consequently, the $PbBr_2$ phase is not totally removed in the $MAPbBr_3$ layers formed from $PbBr_2$ films.

The surface morphologies of the different perovskite samples on mp-TiO_2 were characterized by registering the SEM images. Fig. 4 shows the top view of images of the three lead halide precursors ($PbCl_2$, $PbBr_2$ and PbI_2) and the corresponding $MAPbBr_3$ films formed upon reaction with a solution of MABr for 10 min. Clear differences in the crystal morphology were observed and whereas $PbCl_2$ and $PbBr_2$ salts were deposited just inside the TiO_2 pores, a non-continuous capping layer on top of TiO_2 was formed with PbI_2. The samples were prepared in exactly the same way independently of the salt (with a small variation for $PbCl_2$ deposition), and consequently, as the salts were different, differences were observed between the deposited layers that influence the final $MAPbBr_3$ layer obtained. In this sense, whereas $MAPbBr_3$ prepared from $PbCl_2$ crystallizes inside the porous TiO_2, for PbI_2 and $PbBr_2$ precursors a non-continuous capping layer of $MAPbBr_3$ can be seen on the top, and this indicated a greater filling of the pores with $PbBr_2$ in comparison with $PbCl_2$. The slight differences observed in the palette of yellow color for $MAPbBr_3$ after a dipping process of 10 minutes, see Fig. 1, can be attributed to the thickness difference because of the presence of the perovskite overlayer (Fig. 4), to the presence of a $PbBr_2$ phase for the perovskite obtained from this lead precursor (Fig. 2) and to the different stoichiometry of the perovskite layers (Fig. 3). A variation of the growth conditions can cause the production of a layer with just perovskite embedded in the TiO_2 scaffold or the preparation of a layer with a capping of perovskite on top of the TiO_2 scaffold.[32] Using the appropriate growth conditions for $PbCl_2$ and $PbBr_2$ would provide samples with a capping layer, but here it was preferred to just compare the samples in terms of different materials and not in terms of different material and different growth conditions.

The UV-vis absorption spectra in Fig. 5 showed the light absorption properties of the perovskite films although this depended on the lead precursors and the time of dipping. Fig. 5a shows the absorption spectra of the PS films with the shortest reaction time (40 s) and clear variations of the wavelength corresponding to the absorption onset were observed depending on the precursor employed: 498 nm for $PbCl_2$, 557 nm for $PbBr_2$ and 588 nm for PbI_2. The onset wavelength was calculated from the extrapolation of the absorption spectrum and the corresponding interception with the abscissa axis. It was quite clear that after 10 min of reaction (Fig. 5b) the sample prepared from $PbCl_2$ suffered a red-shift of 68 nm (from 449 nm to 517 nm at dipping times of 40 s and 10 min, respectively), which indicated its transformation into all-bromide perovskite. However, the absorption onset for samples prepared from PbI_2 suffers a blue-shift of 30 nm (from 556 nm to 526 nm) and no significant shift is observed for those prepared from $PbBr_2$ over the different reaction times (from 519 nm to 522 nm). The similar absorption onset of the three types of samples after 10 min of reaction time indicated that $MAPbBr_3$ crystals were being formed, after a sufficient reaction time, regardless of the nature of the lead halide precursor, and these results were in good agreement with those of the XRD experiments.

It is well known that the ability of the halide anion to tune the bandgap of the corresponding perovskite crystals depends on their composition,[20,33,34] where chloride perovskites show the largest bandgap, E_g, and this decreases progressively for bromide and iodide perovskites ($MAPbCl_3$ > $MAPbBr_3$ > $MAPbI_3$).

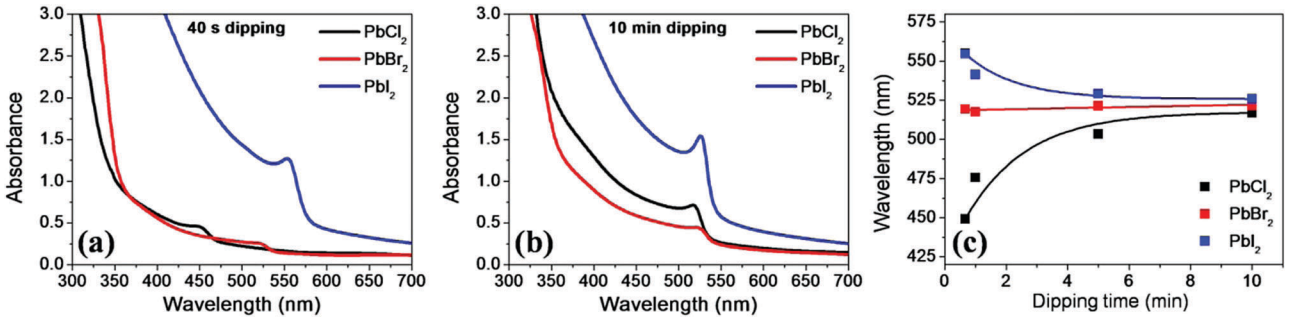

Fig. 5 UV-vis spectra of perovskite films with different lead precursors of $PbCl_2$, $PbBr_2$ and PbI_2 (a) at 40 s, (b) at 10 min and (c) at different times of dipping: 40 s, 1 min, 5 min and 10 min.

Fig. 5c shows the evolution of the absorption onset with the dipping time. The light absorption measurements of the initial PbX_2 salt layers and the evolution of each one at different dipping times are plotted in Fig. S3 (ESI†). It is also important to highlight that the excitonic absorption peak is clearly visible for $MAPbBr_3$ samples formed from $PbCl_2$ and especially from PbI_2 (Fig. 5b).

Very interesting conclusions about the structural evolution of the samples analyzed can be also extracted from an accurate analysis of the PL. The normalized PL spectra of the samples studied are shown in Fig. 6. Fig. 6a–c show the evolution of the emission spectra of the films resulting from the corresponding PbI_2, $PbBr_2$ and $PbCl_2$ precursors, respectively, with varying dipping times. For samples using the PbI_2 salt two clearly separated emission peaks are observed after just 40 s of dipping, see Fig. 6a. The strongest PL peak is observed at longer wavelengths, such as 728 nm, whereas a smaller peak is observed at 538 nm. The peak in the green spectral region (538 nm) can be associated to the $MAPbBr_3$ perovskite, thus indicating the formation of this perovskite at a very early stage, and this result is in good agreement with that obtained using XRD. The peak at longer wavelengths is associated with $MAPb(Br_{1-x}I_x)_3$ perovskite with a high iodide content close to $MAPbI_3$. However, the weight of this phase has to be very low as it was not detected using XRD (Fig. 2b). The higher emission peak arising for the radiative recombination of this phase can be explained by the band alignment that produces a change transfer to the phase with the lower bandgap.[35] Emission from $MAPb(Br_{1-x}I_x)_3$ was reduced with the dipping time and after 10 minutes of reaction, just the emission from $MAPbBr_3$ could be observed. The presence of this phase is also responsible for the orange color observed for samples prepared with PbI_2 precursors and with low dipping times (Fig. 1).

For the $PbBr_2$ precursor no significant changes were observed in the PL spectra over the reaction time (Fig. 6b), because the only possible composition of the resulting PS is $MAPbBr_3$ whose emission maxima is centered at 535 nm after 10 min of reaction. For $PbCl_2$ at the shortest reaction time, a broad emission signal with two maxima centered at 412 and 468 nm, respectively, was observed (Fig. 6c). The multiple emission signal is ascribed to the presence of different perovskite domains with different compositions, *i.e.*, $MAPbCl_{3-x}Br_x$ with a variable Br^-/Cl^- ratio, and these results are in good agreement with those obtained using XRD and light absorption measurements. As long as the dipping time increases, a systematic red-shift of the PL spectra was observed and the multiple emission signal was red-shifted and converted into a single signal centered at 517 nm. It is worth noting that those samples prepared from the different lead precursors ($PbCl_2$, $PbBr_2$ and PbI_2) with 10 min of reaction, showed slight variations of emission maxima position, *i.e.*, 517 nm for $PbCl_2$, and 536 nm for $PbBr_2$ and PbI_2. This was probably because of the significant differences in the crystal size and a blue shift of PL emission was reported with the decrease of grain size.[15,36] $MAPbBr_3$ grown from $PbCl_2$ presents a lower average grain size, because it crystallizes inside the TiO_2 pores, and the size of perovskite grains cannot be larger than the size of the TiO_2 nanoparticles, which is $\sim$30 nm. However, the grain size of the perovskite over layer on top of the mp-TiO_2 grown from $PbBr_2$ and PbI_2 was several hundreds of nanometers (Fig. 4).

Finally, photovoltaic devices were fabricated with the $MAPbBr_3$ layers obtained. The *J–V* curves of the three devices developed from the three different lead precursors $PbCl_2$, $PbBr_2$ and PbI_2 with 10 min reaction with MABr, are given in Fig. 7a and the average cell performance parameters are summarized in Table 1. Note that all three salts have been prepared following the same procedure without any particular optimization for each material and therefore, the solar cell performance is far away from being optimized. However, an important conclusion can be extracted about the effect of the different halide salts for the preparation of $MAPbBr_3$ perovskite. The most remarkable feature, as shown in Table 1, is the strong dependence of the solar cell parameters, short circuit current (J_{sc}), FF, and open circuit potential (V_{oc}) on the PbX_2 salt employed for the synthesis of $MAPbBr_3$. From Fig. 3 it can be observed that the perovskite sample prepared from $PbBr_2$ salt presents a Br/Pb ratio close to 3, the value expected for perovskites, whereas samples obtained from the other halide salts were halide rich films with higher ratios. This fact could explain the increase in photocurrent detected for samples prepared from $PbBr_2$. However, this hypothesis needs further confirmation. A systematic optimization of the growth conditions in each case is required to determine whether the higher photocurrent is just a consequence of the non-optimized deposition method or if it arises from a structural reason as commented previously.

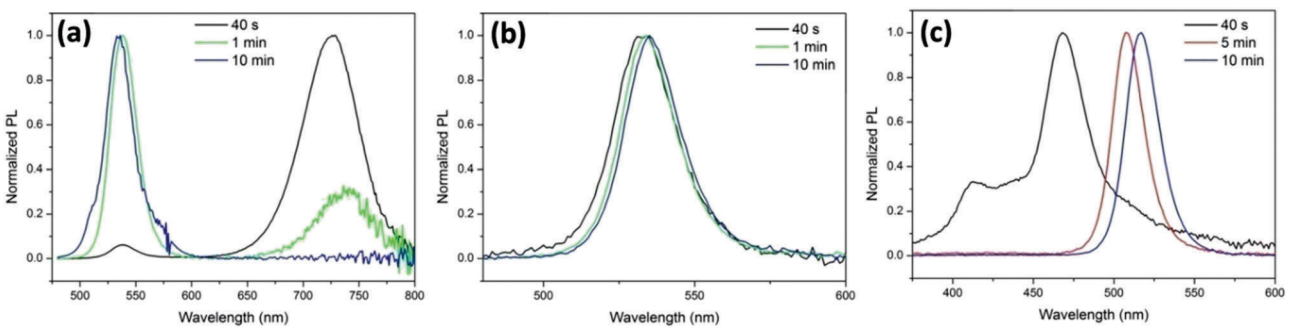

Fig. 6 Normalized PL spectra of the films shown in Fig. 1, at different dipping times for the different lead halide precursors (a) PbI_2, (b) $PbBr_2$ and (c) $PbCl_2$.

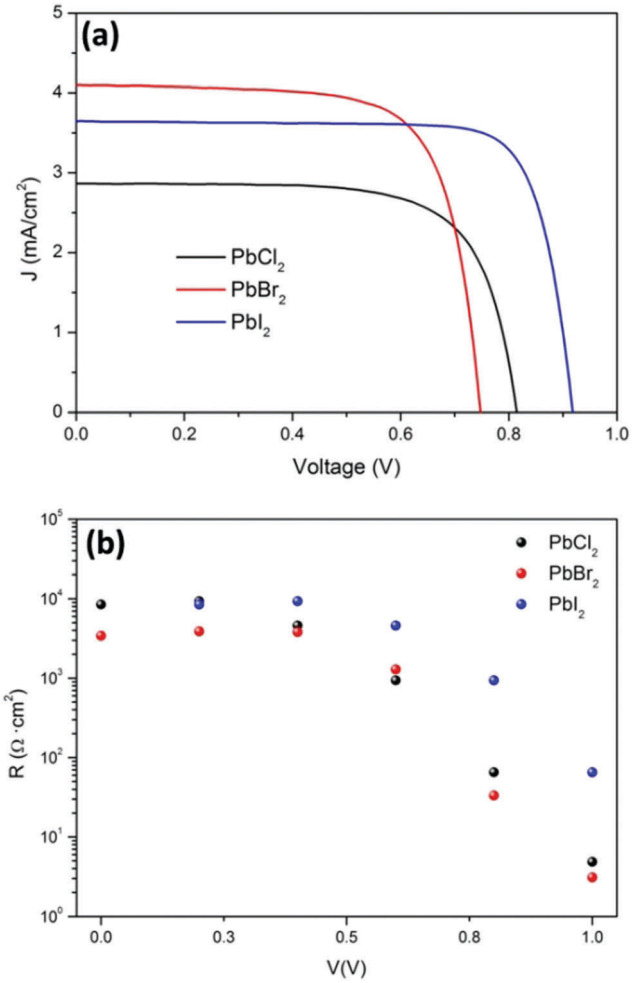

Fig. 7 (a) J–V curves of the devices developed with the three different lead precursors PbI_2, $PbBr_2$ and $PbCl_2$, dipped for 10 min in the MABr solution. (b) Recombination resistance obtained for the same samples using IS.

Table 1 Average photovoltaic performance of the perovskite-based devices with the standard deviation in parentheses, and results for the champion cell. The device architecture was FTO/c-TiO_2/mp-TiO_2/PS/Spiro-OMeTAD/Au

Lead precursor	J_{sc} (mA cm^{-2})	V_{oc} (V)	FF (%)	PCE (%)
$PbCl_2$	2.96 (±0.13)	0.79 (±0.04)	67.8 (±1.0)	1.58 (±0.05)
$PbBr_2$	4.05 (±0.24)	0.72 (±0.01)	71.9 (±0.8)	2.11 (±0.16)
PbI_2	2.9 (±0.5)	0.94 (±0.02)	77.1 (±2.4)	2.1 (±0.4)
PbI_2 champion	3.65	0.92	79.4	2.7

Short-circuit current density (J_{sc}), open circuit voltage (V_{oc}), fill factor (FF) and power conversion efficiency (PCE).

Furthermore, the variation of V_{oc} is easier to determine at this preliminary optimization stage. For this purpose IS analysis of the solar cells prepared from the three different lead salts was carried out. The V_{oc} of these cells depended on the lead precursor employed, being on average 0.72 V for $PbBr_2$, 0.79 V for $PbCl_2$ and 0.94 V for PbI_2. IS spectra have been fitted using the previously reported equivalent circuit.[37] IS has been broadly used for the characterization of PSC.[20,37–40] Fig. 7b plots the resistance of the low frequency arc that has been related to the recombination resistance[20,38–40] and consequently, is inversely proportional to the recombination rate. It can be seen that the resistance (Fig. 7b), especially for applied potentials close to V_{oc}, depended on the lead precursor as PbI_2 > $PbCl_2$ > $PbBr_2$, was the trend obtained for V_{oc} (see Fig. 7a and Table 1). In fact, the champion cell with 2.7% photoconversion efficiency was obtained using the PbI_2 salt (Table 1). These results point to a lower recombination rate for samples grown using $PbCl_2$ and especially PbI_2.

A good photovoltaic material is also a good light emitter as radiative recombination cannot be removed.[41] As the photon absorption is allowed (in fact it is the basis of the photovoltaic process) the reciprocal process (the photoexcited carrier recombination emitting a photon) is also possible because of the reciprocity principle.[42] In a real device, in addition to ideal radiative recombination there are alternative non-radiative recombination pathways that can be removed by optimization of the system. Consequently, the disappearance of the fast and avoidable non-radiative recombination produces an increase of the unavoidable radiative recombination pathway with a subsequent increase of PL. The intensity of the PL emitted for the different samples [Fig. S4 (ESI†)], also scales as PbI_2 > $PbCl_2$ > $PbBr_2$, thus pointing to the same direction of reduced non-radiative recombination of $MAPbBr_3$ prepared from $PbCl_2$ and especially PbI_2 compared to the one prepared from $PbBr_2$. Probably the presence of unreacted $PbBr_2$, as was detected using XRD (see Fig. 2b), was producing alternative non-radiative recombination pathways. In addition, as has been previously commented, $MAPbBr_3$ obtained from PbI_2 and $PbCl_2$ are halide rich samples and consequently the presence of metallic Pb, associated with recombination centers, is lower.[3,43] The higher V_{oc} has the additional beneficial effect of increasing the FF.[44]

Conclusion

The perovskite $MAPbBr_3$ material was successfully developed starting from different lead precursor layers: $PbCl_2$, $PbBr_2$ and PbI_2. The absorption and the emission of the perovskite films could be easily controlled by managing the dipping time and exploiting the classical two-step method, which is based on the spin-coating deposition of the lead halide precursor and subsequent dipping in a MABr solution. However, the $MAPbBr_3$ material is produced after a long enough dipping time regardless of the starting precursor, and the properties of these layers are strongly dependent on the precursor employed. This fact was highlighted by the preparation of solar cells. Solar cells prepared from PbI_2 or $PbCl_2$ were halide rich and show higher PL and V_{oc}, thus pointing to a reduction of the non-radiative charge recombination, especially for PbI_2. These results highlight the importance of the choice of the corresponding precursors for the development of high efficiency solar cells. The higher recombination detected in $MAPbBr_3$ prepared from $PbBr_2$ can be attributed to the presence of a mixed phase containing both $MAPbBr_3$ and $PbBr_2$, whereas surprisingly for $PbCl_2$ and PbI_2, the layers were

fully transformed into $MAPbBr_3$, as has been detected by the XRD analysis. Furthermore, the reduction of metallic recombination centers in the halide-rich perovskites (the ones produced from PbI_2 or $PbCl_2$ salts) could contribute to the recombination reduction. In addition to the potential for the preparation of photovoltaic devices, the materials and procedures analyzed in this research could constitute an excellent platform for the study of ion migration and defect formation, and their effects on the properties of halide perovskite materials.

Acknowledgements

The authors wish to thank the Tunisian Ministry of Higher Education and Scientific Research (MHESR) for the financial support of this work. The work was supported by MINECO of Spain (Projects MAT2016-76892-C3-1-R and MAT2015-70611-ERC) and by Generalitat Valenciana (Project PROMETEOII/2014/020). We acknowledge SCIC from the University Jaume I for help with the XRD and SEM characterization. BCH is grateful to the support of the National Council of Technological and Scientific Development (CNPq), Brazil, through the Science without Borders program.

References

1 J. Burschka, N. Pellet, S.-J. Moon, R. Humphry-Baker, P. Gao, M. K. Nazeeruddin and M. Gratzel, *Nature*, 2013, **499**, 316–319.
2 W. S. Yang, J. H. Noh, N. J. Jeon, Y. C. Kim, S. Ryu, J. Seo and S. I. Seok, *Science*, 2015, **348**, 1234–1237.
3 H. Cho, S.-H. Jeong, M.-H. Park, Y.-H. Kim, C. Wolf, C.-L. Lee, J. H. Heo, A. Sadhanala, N. Myoung, S. Yoo, S. H. Im, R. H. Friend and T.-W. Lee, *Science*, 2015, **350**, 1222–1225.
4 Y. Zhao, A. M. Nardes and K. Zhu, *Faraday Discuss.*, 2014, **176**, 301–312.
5 N.-G. Park, *J. Phys. Lett.*, 2013, **4**, 2423–2429.
6 C. C. Stoumpos, C. D. Malliakas and M. G. Kanatzidis, *Inorg. Chem.*, 2013, **52**, 9019–9038.
7 E. Edri, S. Kirmayer, M. Kulbak, G. Hodes and D. Cahen, *J. Phys. Lett.*, 2014, **5**, 429–433.
8 E. Edri, S. Kirmayer, D. Cahen and G. Hodes, *J. Phys. Lett.*, 2013, **4**, 897–902.
9 R. E. Beal, D. J. Slotcavage, T. Leijtens, A. R. Bowring, R. A. Belisle, W. H. Nguyen, G. F. Burkhard, E. T. Hoke and M. D. McGehee, *J. Phys. Lett.*, 2016, **7**, 746–751.
10 D. P. McMeekin, G. Sadoughi, W. Rehman, G. E. Eperon, M. Saliba, M. T. Hörantner, A. Haghighirad, N. Sakai, L. Korte, B. Rech, M. B. Johnston, L. M. Herz and H. J. Snaith, *Science*, 2016, **351**, 151–155.
11 B. R. Sutherland and E. H. Sargent, *Nat. Photonics*, 2016, **10**, 295–302.
12 S. A. Veldhuis, P. P. Boix, N. Yantara, M. Li, T. C. Sum, N. Mathews and S. G. Mhaisalkar, *Adv. Mater.*, 2016, **28**, 6804–6834.
13 H.-S. Kim, C.-R. Lee, J.-H. Im, K.-B. Lee, T. Moehl, A. Marchioro, S.-J. Moon, R. Humphry-Baker, J.-H. Yum, J. E. Moser, M. Gratzel and N.-G. Park, *Sci. Rep.*, 2012, **2**, 591.
14 M. M. Lee, J. Teuscher, T. Miyasaka, T. N. Murakami and H. J. Snaith, *Science*, 2012, **338**, 643–647.
15 F. K. Aldibaja, L. Badia, E. Mas-Marza, R. S. Sanchez, E. M. Barea and I. Mora-Sero, *J. Mater. Chem. A*, 2015, **3**, 9194–9200.
16 S. D. Stranks, G. E. Eperon, G. Grancini, C. Menelaou, M. J. P. Alcocer, T. Leijtens, L. M. Herz, A. Petrozza and H. J. Snaith, *Science*, 2013, **342**, 341–344.
17 S. Dharani, H. A. Dewi, R. R. Prabhakar, T. Baikie, C. Shi, D. Yonghua, N. Mathews, P. P. Boix and S. G. Mhaisalkar, *Nanoscale*, 2014, **6**, 13854–13860.
18 Y. Zhao and K. Zhu, *J. Phys. Chem. C*, 2014, **118**, 9412–9418.
19 C. Ludmila, U. Satoshi, J. A. Kumar, M. Tsutomu, N. Jotaro, K. Takaya and S. Hiroshi, *Chem. Lett.*, 2015, **44**, 1089–1091.
20 B. Suarez, V. Gonzalez-Pedro, T. S. Ripolles, R. S. Sanchez, L. Otero and I. Mora-Sero, *J. Phys. Chem. Lett.*, 2014, **5**, 1628–1635.
21 D. W. de Quilettes, S. M. Vorpahl, S. D. Stranks, H. Nagaoka, G. E. Eperon, M. E. Ziffer, H. J. Snaith and D. S. Ginger, *Science*, 2015, **348**, 683–686.
22 Q. A. Akkerman, V. D'Innocenzo, S. Accornero, A. Scarpellini, A. Petrozza, M. Prato and L. Manna, *J. Am. Chem. Soc.*, 2015, **137**, 10276–10281.
23 J. B. Hoffman, A. L. Schleper and P. V. Kamat, *J. Am. Chem. Soc.*, 2016, **138**, 8603–8611.
24 G. Nedelcu, L. Protesescu, S. Yakunin, M. I. Bodnarchuk, M. J. Grotevent and M. V. Kovalenko, *Nano Lett.*, 2015, **15**, 5635–5640.
25 G. Li, J. Y.-L. Ho, M. Wong and H. S. Kwok, *J. Phys. Chem. C*, 2015, **119**, 26883–26888.
26 D. Solis-Ibarra, I. C. Smith and H. I. Karunadasa, *Chem. Sci.*, 2015, **6**, 4054–4059.
27 N. Pellet, J. Teuscher, J. Maier and M. Grätzel, *Chem. Mater.*, 2015, **27**, 2181–2188.
28 Y. Zhao and K. Zhu, *J. Am. Chem. Soc.*, 2014, **136**, 12241–12244.
29 C. Eames, J. M. Frost, P. R. F. Barnes, B. C. O'Regan, A. Walsh and M. S. Islam, *Nat. Commun.*, 2015, **6**, 7497.
30 J. M. Azpiroz, E. Mosconi, J. Bisquert and F. De Angelis, *Energy Environ. Sci.*, 2015, **8**, 2118–2127.
31 W.-J. Yin, T. Shi and Y. Yan, *Appl. Phys. Lett.*, 2014, **104**, 063903.
32 A. Listorti, E. J. Juarez-Perez, C. Frontera, V. Roiati, L. Garcia-Andrade, S. Colella, A. Rizzo, P. Ortiz and I. Mora-Sero, *J. Phys. Lett.*, 2015, **6**, 1628–1637.
33 *G. E. Eperon*, *S. D. Stranks*, *C.* Menelaou, M. B. Johnston, L. M. Herz and H. J. Snaith, *Energy Environ. Sci.*, 2014, **7**, 982–988.
34 J. H. Noh, S. H. Im, J. H. Heo, T. N. Mandal and S. I. Seok, *Nano Lett.*, 2013, **13**, 1764–1769.
35 E. T. Hoke, D. J. Slotcavage, E. R. Dohner, A. R. Bowring, H. I. Karunadasa and M. D. McGehee, *Chem. Sci.*, 2015, **6**, 613–617.

36 V. D'Innocenzo, A. R. Srimath Kandada, M. De Bastiani, M. Gandini and A. Petrozza, *J. Am. Chem. Soc.*, 2014, **136**, 17730–17733.
37 A. Guerrero, G. Garcia-Belmonte, I. Mora-Sero, J. Bisquert, Y. S. Kang, T. J. Jacobsson, J.-P. Correa-Baena and A. Hagfeldt, *J. Phys. Chem. C*, 2016, **120**, 8023–8032.
38 A. Dualeh, T. Moehl, N. Tétreault, J. Teuscher, P. Gao, M. K. Nazeeruddin and M. Grätzel, *ACS Nano*, 2014, **8**, 362–373.
39 E. J. Juarez-Perez, M. Wuβler, F. Fabregat-Santiago, K. Lakus-Wollny, E. Mankel, T. Mayer, W. Jaegermann and I. Mora-Sero, *J. Phys. Chem. Lett.*, 2014, **5**, 680–685.
40 A. Pockett, G. E. Eperon, T. Peltola, H. J. Snaith, A. Walker, L. M. Peter and P. J. Cameron, *J. Phys. Chem. C*, 2015, **119**, 3456–3465.
41 O. D. Miller, E. Yablonovitch and S. R. Kurtz, *IEEE J. Photovoltaics*, 2012, **2**, 303–311.
42 W. Shockley and H. J. Queisser, *J. Appl. Phys.*, 1961, **32**, 510–519.
43 I. A. Shkrob and T. W. Marin, *J. Phys. Chem. Lett.*, 2014, **5**, 1066–1071.
44 F. Fabregat-Santiago, G. Garcia-Belmonte, I. Mora-Seró and J. Bisquert, *Phys. Chem. Chem. Phys.*, 2011, **13**, 9083–9118.